2020-04-15

Oil-mineral flocculation and settling velocity in saline water

Ye, L

10.1016/j.watres.2020.115569
Water Research
Elsevier BV

Oil-Mineral Flocculation and Settling Velocity in Saline Water

Leiping Ye[a,*], Andrew J. Manning[a,b,c], Tian-Jian Hsu[a]

[a] *Center for Applied Coastal Research, Department of Civil and Environmental Engineering, University of Delaware, Newark, DE 19716, United States*

[b] *HR Wallingford Ltd., Coasts and Ocean Group, Wallingford OX10 8BA, United Kingdom*

[c] *School of Biological and Marine Sciences, University of Plymouth, Plymouth PL4 8AA, United Kingdom*

[*] *Corresponding author: Tel: +1 302-763-6502; Email: lye@udel.edu*

Abstract

Cohesive particles in aquatic systems can play an important role in determining the eventual fate of spilled oil via the generation of Oil-Mineral Aggregates (OMAs). Series of laboratory experiments have been conducted aiming at filling the knowledge gap regarding how cohesive clay particles influence the accumulation of petroleum through forming different aggregate structures and their resulting settling velocity. OMAs have been successfully created in a stirring jar with artificial sea-water, crude oil and two types of most common natural cohesive minerals, Kaolinite and Bentonite clay. With the magnetic stirrer adjusted to 490 rpm to provide a high level homogeneous flow turbulence (Turbulence dissipation ϵ estimated to be about 0.02 $\mathrm{m^2 \cdot s^{-3}}$), droplet OMAs and flake/solid OMAs have been obtained in oil-Kaolinite sample and oil-Bentonite sample, respectively. Kaolinite clay with relatively low flocculation rate ($R_f = 0.13$ $\mathrm{min^{-1}}$) tends to physically

attach around the surface of oil droplets. With the lower density of oil, these oil-Kaolinite droplet OMAs generally show lower settling velocity comparing to pure mineral Kaolinite flocs. Differently, Bentonite clay with higher flocculation rate ($R_f = 0.66$ min^{-1}) produces high porous flocs that can absorb or be absorbed by the oil and form compact flake/solid OMAs with higher density and settling velocity than pure Bentonite flocs. Some of the large oil-Bentonite OMAs are measured to have settling velocities up to 10 mm·s^{-1}. In the mixture condition (Kaolinite:Bentonite = 1:1 in weight), oil can be considered to preferably interacting with Bentonite. The microflocs (< 160 μm) are dominated by Kaolinite with lower oil participation and lower settling velocity, but the Macroflocs (> 160 μm) which dominates the entire sample's average properties are more influenced by the oil-Bentonite characteristics.

Keywords: Oil-Mineral Aggregates (OMAs), settling velocity, microfloc, Macrofloc.

1. Introduction

Since the petroleum exploration and transportation became one of the most critical industrial activities for the global economic growth, extremely large oil spill disasters, such as the 1989 Exxon Valdez spill (0.26 million barrels of oil released to Alaska's Prince William Sound) (Peterson et al., 2003) and the 2010 Deepwater Horizon (DWH) disaster (4.9 million barrels of oil were released into the Gulf of Mexico) (Crone and Tolstoy, 2010; At-

las and Hazen, 2011), and increasingly smaller size spills occurred in the coastal zones (Hayakawa et al., 2006; Doshi et al., 2018; Liu and Callies, 2019). These oil spill accidents pose detrimental impacts on sea-based human activities(Peterson et al., 2003), ecosystem contamination of aquatic bio-communities (Ainsworth et al., 2018) such as fishes (Murawski et al., 2014), birds (Henkel et al., 2012), coral (White et al., 2012) or plankton (Almeda et al., 2013, 2016). Although most mitigation methods focus on spilt oil floating onto the water surface (Reddy et al., 2002, 2012; Liu et al., 2012), there can be a considerable portion of spilt oil settles to the sea-floor after flocculating with natural cohesive materials, including sediments and organic particles (Chanton et al., 2014; Yan et al., 2016; Jones and Bridgeman, 2016; Romero et al., 2017; O'Laughlin et al., 2017).

Flocculation with cohesive mineral sediments can be especially common in more energetic coastal environments where resuspension of sediment is more likely or near river mouths where new supplies of sediments are abundant (Strom and Keyvani, 2016; Shen et al., 2018). When crude oil is released into aquatic systems in nature, oil droplets can be open to flocculate with suspended particles (Sterling Jr et al., 2005). Through settling and deposition, the oil mineral aggregates may eventually preserving in the sea-floor depositions over geological time (Romero et al., 2017). Therefore, the interactions of oil and aquatic mineral particles, or biological materials can play an important role in the fate of spilt oil (Khelifa et al., 2002, 2005a; Passow and Hetland, 2016; O'Laughlin et al., 2017). This study focuses on

the influence of mineral sediments on oil droplets through flocculation. Some insights into the flocculation of oil droplets with biological materials, namely the marine snows, can be found in, for instance, Passow et al. (2012) and a comprehensive review article of Daly et al. (2016).

Oil droplets tend to aggregate with, and finally be stabilized by, cohesive particles or suspended particle materials (SPM) in the water column and form oil-mineral aggregates (OMAs) (Khelifa et al., 2002), oil-SPM aggregates (OSAs) (Khelifa et al., 2005a) or oil-particle aggregates (OPAs) (e.g., Zhao et al. 2014, 2016, 2017). In the present study, the term "OMAs" has been used because only mineral clay has been utilized to flocculate with oil droplets in the cases. Several earlier studies focus on the structure of OMAs using microscopy imagery and "droplet OMAs", "flake OMAs" or "solid OMAs" are most commonly observed OMA structures (Lee and Stoffyn-Egli, 2001; Stoffyn-Egli and Lee, 2002). Droplet OMAs are combination or enclosure of one or several oil droplet(s) and mineral particles/flocs via surface attachments. On the contrary, flake OMAs have a similar shape as solid OMAs which have membrane-like sheets with an orderly arranged oil and mineral particle configuration (Stoffyn-Egli and Lee, 2002). With higher shear strength, structures of flake OMAs could be altered to become solid OMAs because the crumpling or breaking of flake type OMAs may form more compact and denser floc structures (Stoffyn-Egli and Lee, 2002; Loh et al., 2014). They can be highly compact with oil and mineral absorbed together and organized in dendritic or foldable feather-shape structures.

Later, several important OMAs studies have been focused on the formation mechanisms and influence factors. Omotoso et al. (2002) presented a flocculation index based on the sedimentation behavior of a sheared oil-mineral-water mixture. It was used to quantify the degree of interaction of oil and minerals in water which was found to be dependent on the viscosity of the crude oil and the type of mineral present. On the other hand, Khelifa et al. (2002) suggested that droplet shape and size were not correlated to oil viscosity, but the concentration of oil droplets decreased rapidly with oil viscosity, temperature and asphaltenes-resins content (ARC). Le Floch et al. (2002) quantified the amount of oil incorporated into OMA with the salinity ranging from 0∼35 ppt. They demonstrated that the OMA formation was significantly enhanced by salinity when comparing to distilled water condition. However, the amount of oil contained in OMAs saturated at low salinity of only 2 ppt and further enhancing salinity showed almost no effect OMA formation. This salinity threshold depends on other parameters including oil type and the nature of the mineral present. Below this salinity threshold, there is a linear decrease in the amount of oil incorporated in OMA, to practically zero in distilled water. Hill et al. (2002) presented an equation that defines the time required to coat and stabilize oil droplets with mineral particles suspended in a turbulent medium. The finding that OMA form rapidly given adequate sediment concentration should play a key role in oil spill response decision. With the high demand of quantitative understanding in the formation of OMAs processes, some further laboratory experimental studies

have been reported. Khelifa et al. (2005b) presented the laboratory results showing a positive correlation of OMA sizes and the concentration of mineral-stabilized droplets with salinity positively from zero to a critical aggregation salinity in the range of 1.2∼3.5 ppt. And it is believed that the effect if salinity on droplet size distribution is strongly influenced by clay type. More recently, Sun et al. (2010, 2013) presented the experimental results showing that the formation of oil suspended particle matters aggregates increased exponentially with the mixing time and reached an equilibrium within 4∼5 hours at a provided turbulence dissipation rate of 2.6 $m^2 \cdot s^{-3}$. They believed the shaking rate (turbulence) largely influences the maximum oil trapping efficiency in OMAs. And it is found that most of the formed aggregates were solid aggregates and single droplet aggregates with low mixing energies, and multi-droplet oil suspended particles aggregates with high mixing energies.

Among all the previous OMA literature, very limited studies have been reported to systematically investigate OMAs settling dynamics. Khelifa et al. 2008 reported a series of detailed laboratory experimental jar tests on chemical dispersed oil and natural mixture sediment aggregation. Their data, probably for the first time, showed a direct relationships between the measured settling velocity and OMA size. They suggested that those flocs with low oil concentration may barely change the oil-sediment aggregates behaviors, but with high oil concentration within the oil-sediment aggregates, their density can be much smaller than pure sediment flocs having similar floc sizes. For most sediment types they tested, the effective density of the oil-sediment

aggregates can be about 2∼3 times less than those of pure sediment flocs. Importantly, in their samples, it is suggested that the presence of chemical dispersed oil may enhance the stickiness of sediment grains which helps building up the large flocs with oil participation. More recently, O'Laughlin et al. (2017) reported measured results of dilbit-derived OMAs settling velocity from series of laboratory and wave tank experiments in response to the presence or absence chemical dispersants. They suggested that settling velocities of artificially formed OMAs on the order of 0.1∼0.4 mm·s^{-1}. Moreover, the OMA size, settling velocity and effective particle density were increased in response to the higher concentration of suspended sediment. Their data also show evidences that dispersant may inhibits flocculation. These two studies clearly indicated the importance of cohesion(stickiness) in determining the resulting oil-floc and their settling velocity. As mentioned above, earlier studies also provided very comprehensive understanding on the structures of OMAs. Here, we further hypothesize that a main factor controlling the structures of OMA is the properties of the mineral sediments, for example, their stickiness. Hence, a reasonable next step is to further relate different type of OMA structures with their settling characteristics.

The present study is motivated to investigate the effect of mineral types, which provide different stickiness, in determining the OMA structures and the resulting settling velocities. Data obtained from the controlled laboratory experiments are analyzed with three main objectives: 1) To understand the OMAs structures formed with different types of common clay minerals

by high-resolution digital microscopy, 2) to measure physical characteristics of OMAs, such as their sizes and settling velocities using LabSFLOC-2 camera, and the most importantly 3) synthesize measured data to gain insights into OMA structure and settling dynamics due to different clay types. The remaining of this paper is organized as follow. Section 2 focuses on the laboratory methods, including the OMA generation, turbulence characterization, microscopy and LabSFLOC-2 system for studying settling characteristics. Results are presented in terms of OMA structures and characteristics in Section 3, discussions are in Section 4 and important concluding remarks are in Section 5.

2. Materials and methods

2.1. Laboratory experiment setup

An experimental stand set (Figure 1a) has been designed and a series of magnetic stirring jar experiments have been conducted at the Center for Applied Coastal Research, University of Delaware. White Kaolin clay (92.3±2.5 % Kaolinite), Wyoming sodium Bentonite clay (85.2±2.3 % Montmorillonite) (two most common clay types with large difference in cohesion in saline water) and raw Texas crude oil (Dynamic viscosity: 7.27×10^{-3} Pa·s at 20 °C) with various proportions are used to generate OMAs. As summarized in Table 1, we specify oil-to-sediment ratio close to 2 with clay mineral concentration of 0.5 g per litre of saline water, which provide a condition for maximum OMA formation efficiency condition according to the previ-

ous studies (Guyomarch et al., 2002; Khelifa et al., 2008; Ajijolaiya et al., 2006). Artificial seawater (Salinity $\approx$ 35 ppt) has been made from mixing clean water and pure salt. The jar has a diameter of 11 cm and the flow depth is 13 cm (1 liter salt water). Magnetic stirring speed is set to 490 rpm (Device range: 0$\sim$1000 rpm) for providing the constant turbulence intensity for OMAs generation. Three-component flow velocities are measured by a Vectrino Profiler (Nortek), which was mounted on the shelf above the magnetic stirrer with the sensor probes located 5 cm below the water surface in the jar (in Figure 1a). Flow velocity data was collected without crude oil and sediment but in otherwise the same flow conditions (artificial seawater in the jar with same flow depth). The time series of turbulent velocity fluctuations are transformed into Fourier space to obtain turbulent kinetic energy spectrum. Turbulence dissipation rate is then estimated to be $\epsilon \approx 0.02$ $\mathrm{m^2 \cdot s^{-3}}$ via matching the Kolmogorov spectrum with Taylor frozen turbulence approximation (e.g., Voulgaris and Trowbridge 1998; Huang et al. 2018). The corresponding shear parameter is of seawater (Salinity $\approx$ 35 ppt) at 20 °C (Viscosity $\approx 1.08 \times 10^{-3}$ Pa·s).

Different types of mineral flocs and Oil-Mineral Aggregates (OMAs) samples are generated, including 1) Kaolinite flocs, 2) Bentonite flocs, 3) Mixed Kaolinite-Bentonite flocs, 4) Oil-Kaolinite aggregates, 5) Oil-Bentonite aggregates and 6) Oil-Kaolin-Bentonite aggregates. Each experimental run last up to 2 hours and OMAs are allowed to settle down overnight ($\sim$ 8 hours) which should be long enough for all the particles aggregation and settling.

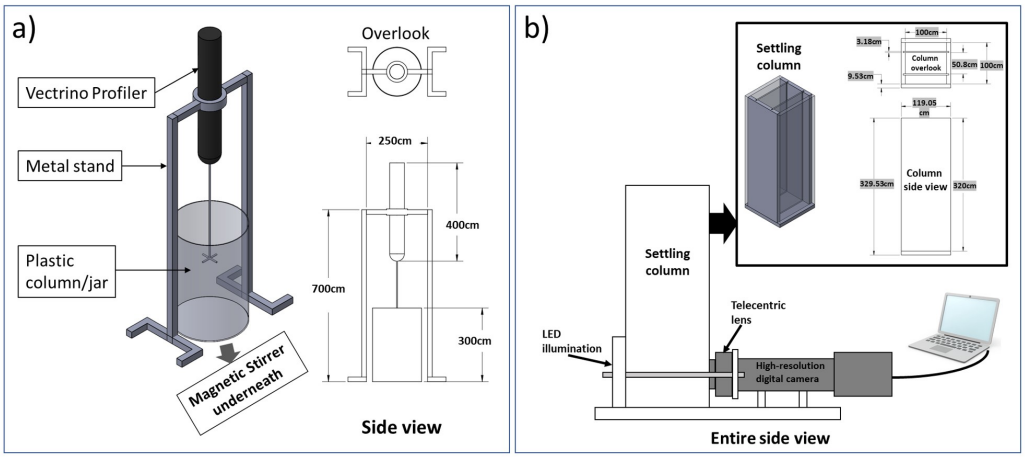

Figure 1: Schematic of the laboratory experimental setup. a) shows the self-designed Vectrino stand set and b) show the LabSFLOC-2 system

Table 1: Various proportions of mineral clay and oil in each experimental run.

Sample	Saline water(L)	Kaolinite clay(g)	Bentonite clay(g)	Texas crude oil(g)
S01	1.00	0.50	/	/
S02	1.00	0.50	/	1.00
S03	1.00	/	0.50	/
S04	1.00	/	0.50	1.00
S05	1.00	0.25	0.25	/
S06	1.00	0.25	0.25	1.00

The mass settling velocity of OMAs were observed using the low intrusive LabSFLOC-2 system (the 2nd version of Laboratory Spectral Flocculation Characteristics instrument) (Figure 1b). This instrument was originally developed by Manning and Dyer (2007) and first used by Gratiot and Manning (2004). It measures the entire floc population for each sample being assessed and has been successfully applied in many cohesive sediment transport studies (Manning et al., 2010; Manning and Schoellhamer, 2013; Uncles and Mitchell, 2017). LabSFLOC-2 utilizes a low-intrusive 2.0 MP Grasshopper monochrome digital video camera to optically observe individual flocs (e.g. Manning and Dyer (2002)) as they settle in a 350 mm high by 100 mm square Perspex settling column. The video camera, positioned nominally 75 mm above the base of the column, views all particles in the center of the column that pass within a 1 mm depth of field, 45 mm from the Sill TZM 1560 high-magnification (5 μm pixel resolution) Telecentric (maximum pixel distortion of 0.6 %), 0.66 (1:1.5) magnification, F4, macro lens fitted behind a 5 mm thick glass faceplate. The LabSFLOC-2 settling column sampling was conducted at the end of each OMA sample's experiment and these OMA samples are believed in an equilibrium stage.

A high-resolution digital microscope system has been used to observe detailed floc structures and to carry out statistical analysis on floc numbers in order to evaluate flocculation rate. All the floc samples were directly collected from the running experiment in real-time using wide mouth (> 2 mm) plastic pipettes to minimize floc disturbance and to transfer the samples from the

mixing jar to the microscope slides without using coverslip to prevent the samples being squeezed. Floc samples are observed with a 4∼10 times zoom-in screen on a DELL laptop by the camera software provided by AmScope Inc.

2.2. Data processing

2.2.1. LabSFLOC-2 camera floc data

As one of the most commonly used floc video camera instruments in estuarine and coastal suspended sediment transport study, the LabSFLOC-2 produces not only visible floc individual images but also other essential quantitative floc properties including floc size, floc shape and floc settling velocity (Manning et al., 2010). Through additional theories, other floc quantities can be derived, such as floc density, fractal dimension and so on. The recorded videos of floc settling videos can be analyzed with Matlab software routines based on the HR Wallingford Ltd DigiFloc software (Benson and Manning, 2013) and Java Script to semi-automatically process the digital recording image stack to obtain floc size and settling velocity spectra (Manning et al., 2010; Uncles and Mitchell, 2017). Using the measured floc diameter D (floc sphere-equivalent diameter), settling velocity W_s, and floc shape, a modified Stokes Law (Stokes, 1851) is used to estimate individual floc effective density (Manning and Schoellhamer, 2013):

$$\rho_e = \frac{18 W_s \beta}{\alpha} \cdot \frac{\rho \nu}{g} \cdot \frac{1 + 0.15 Re^{0.687}}{D^2} \tag{1}$$

in which ρ the is the saltwater density, ν is the kinematic viscosity, g is gravitational acceleration, α and β are shape-related coefficients and they equal to 1 for perfect spheres. Re in the equation is the particle Reynolds number, defined as

$$Re = W_s D/\nu \tag{2}$$

This modified Stokes' Law is used for encountering flocs which have particle Reynolds numbers greater than its original unity. By assuming floc has a fractal structure, the fractal dimension of floc (n_f) can be calculated via the following relationship (Winterwerp and Van Kesteren, 2004):

$$(\frac{D}{d})^{n_f-3} = \frac{\rho_e}{\rho_s - \rho} \tag{3}$$

in which d is the minimum primary particle size which is assumed as ??? (Manning and Schoellhamer (2013)), ρ is the seawater density.

2.2.2. Microscope images analysis

The floc images (e.g., Figure 2a) collected from the digital microscope of each floc sample allow a detailed investigation of floc and OMA structures and the red contours point out the individual flocs which can be manually selected under the screen by real-time observation. Microscope images also provide independent and high-resolution data of floc population, which are number counted manually according to the contours, and shape analyzed for further statistical analysis and flocculation rate evaluation. For each sample,

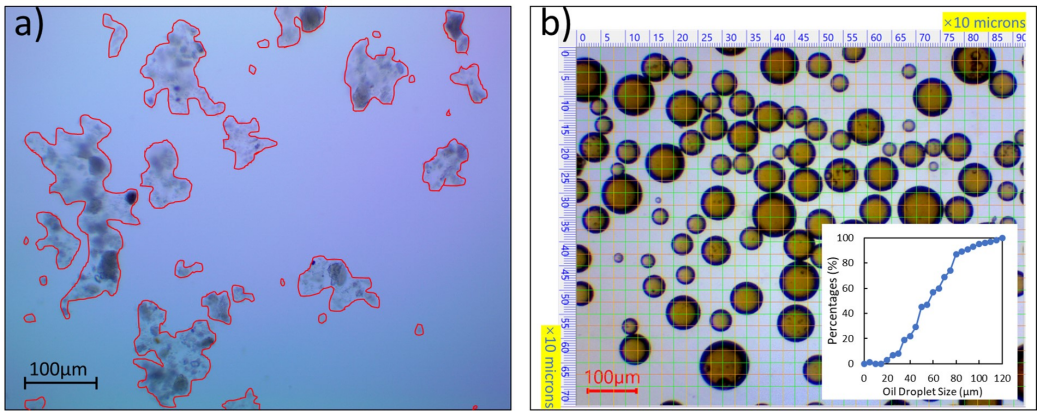

Figure 2: Examples of digital microscope images. a) shows floc number manually counted from a microscope screenshot. The red parts indicate the individual floc can be recognized manually for further statistical analysis. b) shows oil droplets can be manually counted to give the averaged droplet size. The oil droplets are formed and measured after 20 minutes stirring under given turbulence.

six different microscopy images have been analyzed which cover hundreds to thousands individual flocs.

We also use microscope images to calculate averaged oil droplets size under the given turbulence level (e.g., see Figure 2b). The statistical analysis of the pure oil droplets samples images shows the maximum oil droplets size can be up to 120 microns and the mean droplets size is approximately 57 microns. Pure oil droplets size distribution under the constant given turbulence and salinity has been provided in Figure 2b.

2.2.3. Mineral stickiness quantification (Flocculation rate (R_f))

In this study, we quantify the effect of different mineral clays on OMA flocculation by their stickiness. In the study of flocculation with significant organic content, such as due to the presence of transparent exopolymer par-

ticles (TEP) (e.g., Passow (2002)), the stickiness can be quantified by performing experiments to estimate flocculation (efficiency) rate Engel (2000). We perform flocculation rate experiment for three types of mineral particles without the presence of oil, namely cases S01 (Kaolinite), S03 (Bentonite) and S05 (half-half mixture of Kaolinite and Bentonite) (see Table 1), respectively. Temporal microscopy images (six images for each sample at a time) have been collected during mineral flocs development in a magnetic stirrer jar from beginning (0 minute) to the end (2 hours) for each mineral sample. By counting all the floc numbers and normalizing by maximum floc number of each mineral sample which covers hundreds to thousands individual flocs, flocculation evolution time series has been obtained for each type of mineral clay (Figure 3). The manually counted floc numbers cover hundreds to thousands individual flocs which are statistically significant to represent the entire floc distribution and characteristics of each tested sample.

Due to flocculation, the number of particles in each case decays in time. In the semi-logarithmic plot shown in Figure 3, we observed a nearly exponential decay of particle number in the first couple of minutes of the flocculation before the particle number becomes more or less constant in time. By fitting the first three data points in each run, we obtain the representative flocculation rate: R_f. The three trend lines in Figure 3 indicate that Kaolinite clay has the lowest flocculation rate of $R_{f\_Kaolinite} = 0.13$ (min^{-1}) while the Bentonite clay shows a high flocculation rate of $R_{f\_Bentonite} = 0.66$ (min^{-1}) nearly 5 time larger. The mixture of equal amount of Kaolinite and Bentonite

has an intermediate flocculation rate of $R_{f\_mixed} = 0.32$ (min^{-1}). Following Engel (2000), we will consider Kaolinite having the lowest cohesion, followed by the mixture of Kaolinite-Bentonite and Bentonite is among the most cohesive sediments investigated in this study. Noticeably, in the Bentonite (red dots) and mixture (yellow dots) samples, floc numbers increase slightly after reaching the maximum flocculation (lowest normalized floc number) at 5∼6 minutes and reach to equliburium stage after 30 minutes, which may imply the break-up of part of the larger fragile flocs. This indicates that the participant of kaolinite not only reduces the cohesion of pure bentonite, meanwhile, the existence of bentonite weakens the stability of pure kaolinite flocs.

The primary goal of this mineral flocculation rate quantification present here is to compare the difference of stickiness (not floc number) of bentonite and kaolinite because floc numbers between bentonite and kaolin cases have huge difference (bentonite aggregates much larger but less numbers of flocs because of the much higher stickiness) although bentonite sample and kaolin sample have equivalent mineral concentration under same turbulence condition. This information will be shown later to be very useful for the interpretation of the OMA structure and LabSFLOC-2 settling column experimental results.

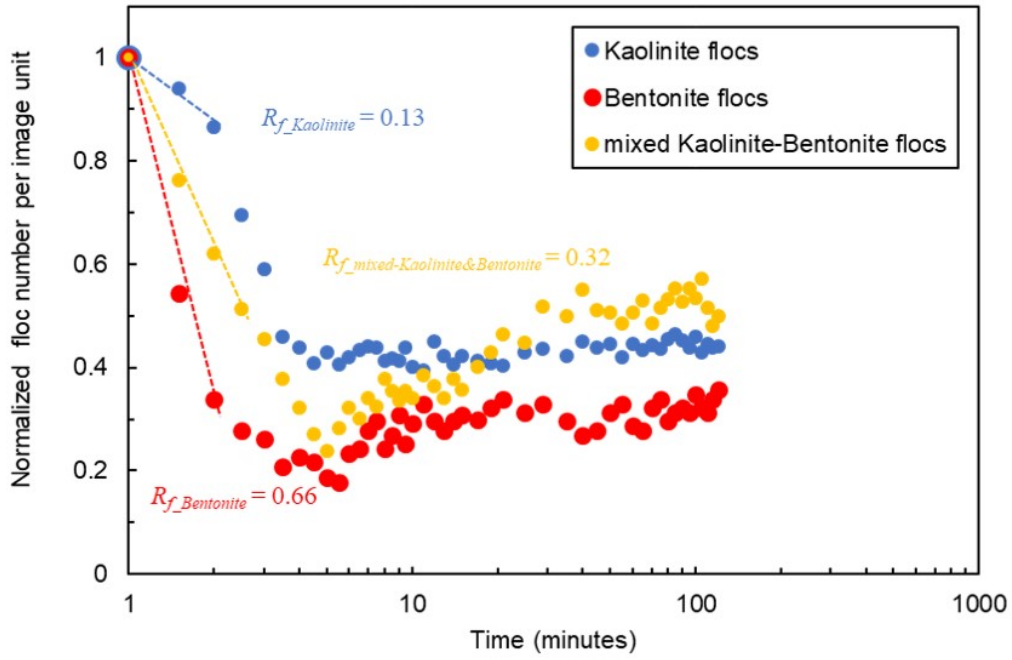

Figure 3: Statistical results of temporal (120 minutes) floc evolutions of normalized floc number for Kaolinite run (blue, S01), Bentonite run (red, S03) and mixed Kaolinite-Bentonite run (yellow, S05). The initial particle number of each run is used for normalization. Each data point comes from manually counted floc number from six different images of each pipette sample which covering hundreds to thousands individual flocs and normalized by the maximum floc number (Kaolinite:1260, Bentonite:782 and Mixture:1323) of each sample.

3. Results

3.1. Floc structures

Samples from each case presented in Table 1 were collected after the flocculation reached equilibrium and have been analyzed by microscopy. High-resolution images provided the details of each mixture floc structure with a magnification factor of 10. Three basic floc types have been observed depending on mineral type: pure mineral flocs/aggregates (no oil) (Figure 4a_1,b_1 & c_1), oil droplets attaching/combining Kaolinite aggregates (Figure 4a_{2-4}), and large flake shaped oil-Bentonite aggregates (Figure 4b_{2-4}).

Figure 4a_1 shows a representative microscope image of settled pure Kaolinite clay flocs (500 mg·l^{-1}, S01 in Table 1). With the addition of 1 g Texas crude oil (S02 in Table 1), the oil droplets can be observed being attached or embraced within the Kaolinite clay structures (such as Figure 4a_{2-4}). The attachment is limited to the surface of oil droplets while the droplets structure remains intact. The oil-Kaolinite aggregates observed are consistent with the droplet OMA type reported in the previous studies (such as Stoffyn-Egli and Lee 2002; Khelifa et al. 2002), in which oil droplets are coated by sediment aggregates through surface attachment. The quantity of mineral attached to a droplet is highly variable.

The OMA obtained from the Bentonite clay run (S03 in Table 1), generated with same turbulent dissipation rate, are shown in Figure 4b_{1-4}. The Bentonite flocs are generally larger than Kaolinite flocs and their size can be up to 100∼200 m in width and several hundred micrometers in length (Figure

345 4b$_1$). These features are distinct from the pure Kaolinite run (S01) shown in
346 Figure 4a$_1$. As demonstrated in section 2.2.3 (or Figure 3), pure Bentonite
347 clay particles are much cohesive and attachable than Kaolinite particles.
348 More importantly, the more cohesive characteristic of Bentonite floc leads
349 to an entirely re-shaped oil-mineral structure (see Figure 4b$_2$, S04 in Table
350 1). Compared with oil-Kaolinite flocs, the sphere-shaped oil droplets disap-
351 peared, and the oil-Bentonite flocs show much larger size of oil soaked mineral
352 having a flake-shaped aggregates up to hundreds of microns in size (see Fig-
353 ure 4b$_{2-4}$). Compared with the previous studies (Stoffyn-Egli and Lee, 2002;
354 Khelifa et al., 2002; Zhao et al., 2016), the dominant oil-Bentonite aggre-
355 gates observed here belong to a dense type of oil-aggregate called flake/solid
356 OMA. Flake aggregates have the appearance of membrane structures, usu-
357 ally floating or neutrally buoyant, which can attain hundreds of microns in
358 length. Their microstructure is highly organized as dendritic or feather-like.
359 Experimental results suggest that high shear strength (i.e. extended or faster
360 agitation) tends to break or crumple flake aggregates. The crumpled flakes
361 (Figure 4b$_{2-4}$) may be distinguished from mineral-embraced droplet OMA
362 (Figure 4a$_{2-4}$) by their folds or preferential orientation of the minerals.

363 After mixing equal amount of Kaolinite and Bentonite clay for Case S05,
364 the mixture flocs contain both Kaolinite floc and Bentonite floc structures
365 (see Figure 4c$_1$), and importantly, although the general size of the mixed
366 flocs (Figure 4c$_1$) are smaller than pure Bentonite case (Figure 4b$_1$). The
367 Bentonite floc structure appears to be dominant in the mixture mineral sam-

ple. With the addition of oil in the mixture sample S06, large flake shaped OMA can be observed in Figure 4f which has similar floc size with those in the oil-Bentonite case (S04, see Figure 4b_{2-4}). However, both droplet OMAs and flake OMAs can be observed (Figure 4c_{3-4}).

Due to different cohesion between Kaolinite and Bentonite clays, the resulting OMA structures are also distinctly different which is expected to lead to different settling velocities. In the next sections, we will investigate different mineral flocs and OMAs settling velocity and discuss their relationship to floc structures.

3.2. Floc physical properties

The previous section provided insights on the floc structures for different types of OMAs by microscopy images. This section is devoted to more quantitative study of floc physical properties, particularly their settling velocities. The scatterplots in Figure 5a, 6a & 7a illustrate individual spherical-equivalent dry mass weighted floc sizes (x-axis) plotted against their corresponding settling velocities (y-axis) of each sample (see Table 1) collected and analyzed by LabSFLOC-2 camera system. The scatterplots allow subsequent statistical analysis for floc properties using 12 different size classes (Size Band details are shown in the bottom of Figure 5-7). The physical properties of particular interest here are, the counted floc numbers of each size band (Figure 5c, 6c & 7c), the settling velocity (Figure 5d, 6d & 7d, floc density (Figure 5e, 6e & 7e) and fractal dimension (Figure 5f, 6f & 7f).

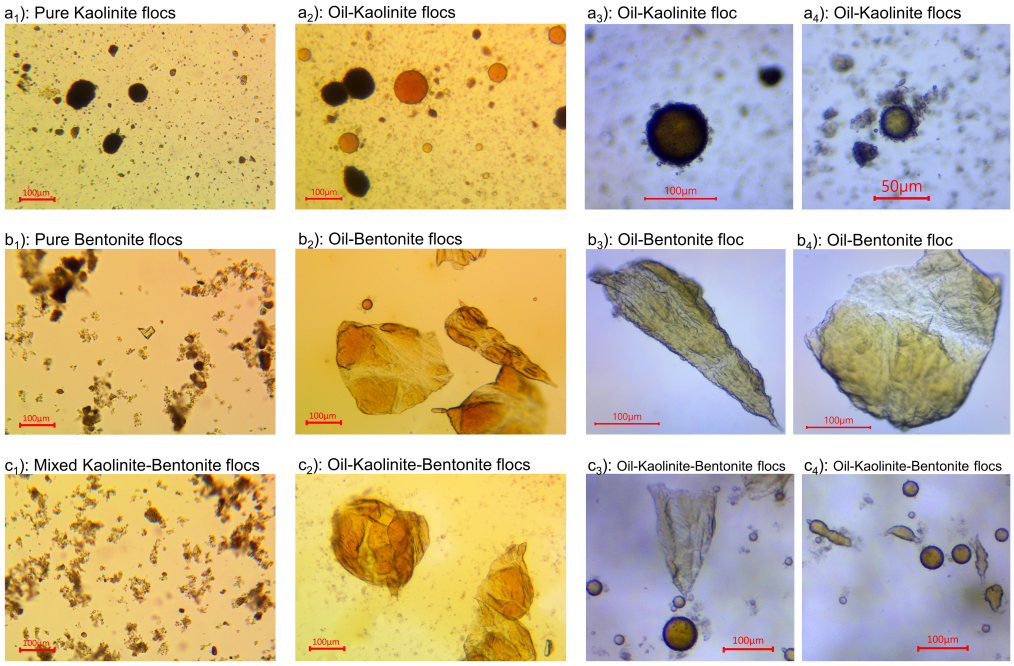

Figure 4: Floc images from the high-resolution digital microscope camera. a1-a4) Kaolinite (S01) and oil-Kaolinite (S02) samples; b1-4) Bentonite (S03) and oil-Bentonite (S04) samples; c1-4) mixed Kaolinite and Bentonite (S05) and oil-Kaolinite-Bentonite (S06) samples.

3.2.1. Kaolinite and Oil-Kaolinite flocs

The scatterplot presented in Figure 5a indicates that the Kaolinite clay flocs (S01) cover a size range from 20 to 400 microns while their settling velocities vary from 0.04 to 10 mm·s^{-1}. Although with some notable scatters, the floc settling velocities are more or less proportional to floc sizes. Adding oil into Kaolinite mineral (S02) shows negligible change in the floc size range (see Figure 5b). However, when floc size is greater than about 80 micron, the peak settling velocities (about 4 mm·s^{-1}) show almost no change with respect to floc size. Also, there exist some low-density flocs in the rather large size range of 200∼400 microns with settling velocities ranging from 0.2∼0.6 mm·s^{-1} (around the red constant density line of 16 kg·m^{-3} in Figure 5b). This is due to the large Oil-Kaolinite flocs having much lower density than those of pure Kaolinite flocs. A more quantitative understanding on these interesting features can be obtained by examining the statistics of 12 size bands.

The number of Kaolinite flocs increases dramatically from Size Band (SB)-1 (20∼40 microns) to SB-3 (80∼120 microns) and then drops quickly from SB-3 to SB-8 (320∼400 microns) (Figure 5c, blue bands). Adding oil to Kaolinite significantly increases floc number for small size flocs (20∼80 microns) at SB-1 and SB-2 while floc numbers at larger size class are generally lower than or similar to those of pure Kaolinite flocs (Figure 5c, orange bars). The settling velocities of Kaolinite samples (S01 and S02 in Table 1) averaged for each size class are shown in Figure 5d. Evidently, pure mineral

flocs (S01) show a rapid increase of settling velocities with respect to the increase of floc sizes for the entire size class spectrum (SB-1 to SB-8). On the contrary, oil-Kaolinite flocs show milder increase of settling velocity with respect to floc size from SB-1to SB-6 until a completely different trend is observed for larger size class (SB-6 to SB-8), namely, a significant decrease of settling velocity with respect to increase of floc size. Overall, adding oil to Kaolinite decreases flocs settling velocity, particularly for larger size classes (by nearly factor 3 in the SB-6 and nearly a factor 7 in the SB-8). Considerable reduction of settling velocity at SB-6 to SB-8 is clearly associated with the significant decrease of floc effective density due to the addition of oil to Kaolinite at this size range (see Figure 5e). Generally, adding oil reduces floc effective density in all size ranges of flocs but the reduction is much more pronounced at large size class. In SB-2 and SB-3, effective density decreases by approximate 1/3 to 1/4 by adding oil while settling velocity also decreases by 1/3 to 1/4. In SB-4 to SB-8, the effective density decreased by half or much more especially in the largest sized flocs, and their settling velocity shows a remarkable reduction in large size flocs such as SB-6 to 8. Since averaged droplet size is about 57 microns as measured in the laboratory tests, it is very likely that there is less oil contained in smaller flocs size classes. Overall, the results presented here is consistent with the presence of oil as droplets (see Figure 4a_2-a_4) having lower density than saltwater or mineral. The low density oil droplets contribute to the reduced settling velocity (or floc density) particularly at the large floc size range.

The fractal dimension for Kaolinite flocs or Kaolinite-oil flocs is in the range of 2.4∼2.6 except for a small number of large flocs in SB-7/8. In general, adding oil slightly reduces fractal dimension to 2.4. A notable exception is that when oil is added to Kaolinite, the largest flocs in SB-8 show a much lower fractal dimension of 2.05 due to containing low density oil droplets in the large structure.

3.2.2. Bentonite and Oil-Bentonite flocs

In the pure Bentonite sample (S03, Figure 6a), we observe some very large size flocs up to 400∼700 microns that do not exist in the pure Kaolinite sample (S01). The resulting settling velocity range is also wider (0.01∼20 $mm{\cdot}s^{-1}$) than that in Kaolinite samples. A more careful examination further suggests that many large size flocs (in SB-9 SB-12 in Figure 6c, 400∼700 microns) in pure Bentonite sample (S03) are of very low density (within 50 $kg{\cdot}m^{-3}$) and their settling velocities are limited to range of 1∼5 $mm{\cdot}s^{-1}$, despite very large floc size. Importantly, adding oil further increased the floc size up to 800 microns (Figure 6b), and it also shows an upper limit of settling velocity but at much higher value of about 10 $mm{\cdot}s^{-1}$ compared to that of oil-Kaolinite (see Figure 5b).

Quantitatively, floc number increases from SB-1 to SB-5 and then reduces afterwards to SB-12 (floc number < 5 in SB-12) (Figure 6c). Comparing to Kaolinite samples (S01 and S02), the most notable difference is that the floc numbers for Bentonite samples are significantly lower than those in Kaoli-

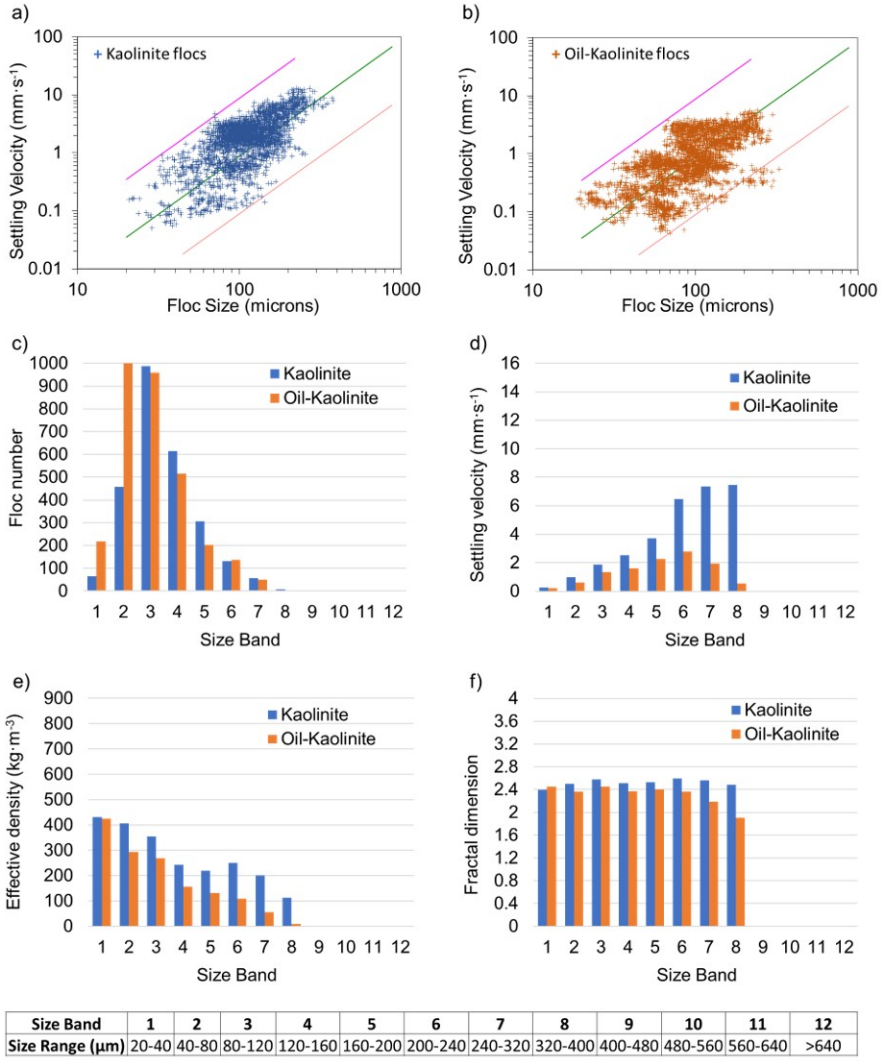

Size Band	1	2	3	4	5	6	7	8	9	10	11	12
Size Range (µm)	20-40	40-80	80-120	120-160	160-200	200-240	240-320	320-400	400-480	480-560	560-640	>640

Figure 5: Floc characteristics from the LabSFLOC-2 analysis. a) & b) show the plots of floc sizes vs. settling velocities of Kaolinite (S01) and Oil-Kaolinite (S02), respectively. The three diagonal lines present contours of Stokes settling velocity calculated with a constant effective density (i.e. floc bulk density minus water density) of 1,600 kg·m^{-3} (pink line, equivalent to a quartz particle), 160 kg·m^{-3} (green) and 16 kg·m^{-3} (red line). c)-f) show the 12 Size Bands trends of floc number, settling velocity, floc density and fractal dimensions respectively for both Kaolinite (blue) and Oil-Kaolinite (orange) samples.

nite sample. Larger floc sizes and lower floc number in Bentonite samples are consistent with the high flocculation rate (high stickiness) of Bentonite discussed in Section 2.2.3. When oil is added to Bentonite (S04) we observe an increase of settling velocities with the floc size (Figure 6d), except at the largest size class (SB-12). This trend is more or less consistent with pure Kaolinite sample (S01, Figure 5d) and Bentonite sample (S03, Figure 6d), but different from the oil-Kaolinite sample (S02, Figure 5d). This suggests that oil interact differently with Kaolinite and Bentonite samples and it is consistent with their distinct droplet OMA and flake OMA structures presented in Figure 4. More importantly, when oil is added to Bentonite, we observe a more rapid increase of settling velocity when floc size increases from SB-9 to SB-12. Furthermore, comparing to the pure Bentonite condition, we obtain an increase of settling velocity by more than a fact of 2 in SB-11, while recall that for Kaolinite samples, adding oil to Kaolinite (S02) significantly reduces the floc settling velocity. These observations are supported by the data from floc effective density. From Figure 6e, we can see that adding oil to Bentonite clay generally increases floc effective density with the most significant increases occur at SB-1 and SB-9 to SB-12 (contrast with Figure 5e, adding oil reduces floc effective density in Kaolinite samples). In this case, the oil droplets no longer exists and become absorbed into mineral flocs. It is likely that at such micro-scale, oil changes the adhesion characteristic and make the small flocs more compact, dense with lower porosity.

The fractal dimension for Bentonite floc or Bentonite-oil flocs are in the

range of 2.2∼2.4 which is slightly lower than those of Kaolinite samples. However, adding oil to Bentonite generally increases fractal dimension with the largest increase occurs at SB-1 with a fractal dimension near 2.5. It is interesting to the point out that, a notable fractal dimension changes after adding oil is in larger size class floc of SB-8 (320∼400 microns) for Kaolinite sample and in the smallest size class of SB-1 (20∼40 microns) for Bentonite sample. This drastic difference is again consistent with different OMA structure of Kaolinite and Bentonite clays.

3.2.3. Mixed Kaolinite-Bentonite and Oil-Kaolinite-Bentonite flocs

In the mixed Kaolinite-Bentonite sample (Figure 7a), a large number of small sized flocs (<80 microns) are observed which are lacking in pure Kaolinite (Figure 5a) or pure Bentonite (Figure 6a) samples. The significant portion of small flocs in SB-12 may due to in the mixture, the kaolinite particles decrease the stickiness of the mixed floc comparing to pure bentonite condition, which may also lead to more small bentonite flocs. Meanwhile, it is likely that the bentonite flocs, when flocculate with kaolinite flocs, make the whole mixed flocs more fragile and with the high turbulence level provided, part of the mixture flocs tends to break-up into smaller flocs, even smaller than those in pure bentonite or kaolinite cases. The observed large amount of microflocs in Figure 7 at the equilibrium stage is consistent with the temporal evolution of normalized floc number shown in Figure 3 that at the later stage, normalized floc number increases. Therefore, when mixing low stickiness

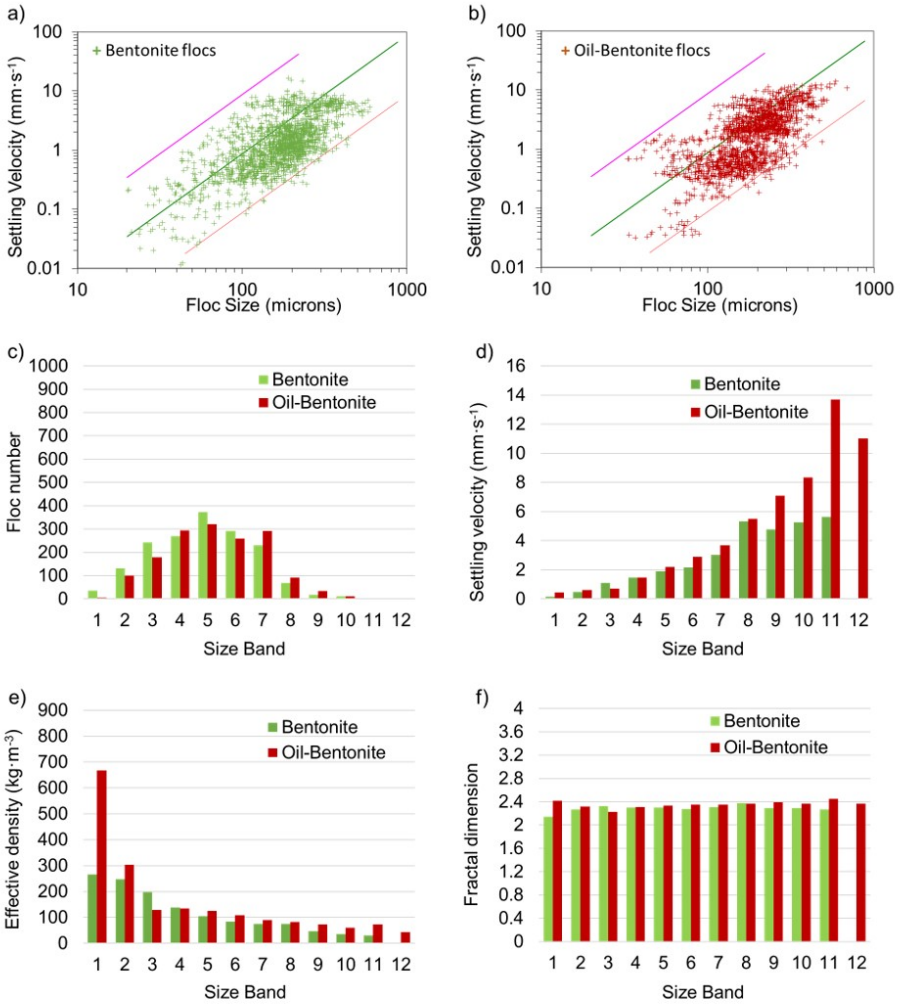

Size Band	1	2	3	4	5	6	7	8	9	10	11	12
Size Range (µm)	20-40	40-80	80-120	120-160	160-200	200-240	240-320	320-400	400-480	480-560	560-640	>640

Figure 6: Floc characteristics from the LabSFLOC-2 analysis. a) & b) show the plots of floc sizes vs. settling velocities of Bentonite (S03) and Oil-Bentonite (S04), respectively. The three diagonal lines present contours of Stokes settling velocity calculated with a constant effective density (i.e. floc bulk density minus water density) of 1,600 kg·m^{-3} (pink line, equivalent to a quartz particle), 160 kg·m^{-3} (green) and 16 kg·m^{-3} (red line). c)-f) show the 12 Size Bands trends of floc number, settling velocity, floc density and fractal dimensions respectively for both Bentonite (blue) and Oil-Bentonite (orange) samples.

kaolinite and high stickiness bentonite, the flocculation process is much more complex and it takes longer time to reach equilibrium. This is because when more porous/fragile bentonite floc structure initially combined with denser kaolinite floc, the entire mixture flocs become fragile to high turbulence and breaks into more small flocs.

The settling velocity for pure Kaolinite-Bentonite flocs peaks at about 10 $mm{\cdot}s^{-1}$ for floc size greater than about 100 microns. When oil is further added to the mixed Kaolinite-Bentonite sample (Figure 7b), we observe even higher settling velocity flocs exceeding 10 $mm{\cdot}s^{-1}$, which is clearly due to higher floc effective density in SB-3 to SB-9 shown in Figure 7e. We also obtain more small flocs but their density is widely spread from nearly close to water (below the red line of 16 $kg{\cdot}m^{-3}$) to those high-density flocs (between the green line of 160 $kg{\cdot}m^{-3}$ and red line of 1600 $kg{\cdot}m^{-3}$).

Generally, both Kaolinite-Bentonite minerals flocs and Oil-Kaolinite-Bentonite flocs show increasing settling velocity with the increasing floc sizes (Figure 7d) except at the largest size class. In other words, by adding oil to equally mixed Kaolinite and Bentonite mixture, the overall settling velocity trend is similar to that of pure Bentonite (Figure 6d). This observation can be further confirmed by examining floc effective density shown in Figure 7e. Similar to adding oil to pure Bentonite (see Figure 6e), adding oil to Kaolinite-Bentonite mixture generally increase floc effective density and hence the settling velocity also increases in most Size Bands. A minor difference is that the rise of settling velocity in SB-9 to SB-12 by adding oil is less dramatic in SB-9

to SB-12 in the Kaolinite-Bentonite mixture case. Also, there is simply less number of those large flocs in Kaolinite-Bentonite mixture cases, suggesting that adding oil to Kaolinite-Bentonite mixture does not increase the cohesion as much when comparing to adding oil to pure Bentonite, possibly due to the presence of less cohesive Kaolinite. Therefore, oil can be considered to preferably interacting with Bentonite and the presence of Kaolinite is of secondary effect to slightly reduce cohesion.

For Kaolinite-Bentonite mixture, the fractal dimension of small sized flocs can be up to 2.8 while the large flocs are of lower value around 2.4 to 2.6. The range of fractal dimension is larger than pure Bentonite (S03) and it is similar to pure Kaolinite (S01) except for the smallest size class (SB-1). By adding oil, flocs fractal dimension in larger size class SB-6 to SB-9 increases and those in small size class SB-1 to SB-5 show negligible change.

3.3. Microflocs and Macroflocs

In the cohesive sediment literature, two distinguished floc components: microflocs and Macroflocs, have been utilized to quantitatively describe the floc spectra (Manning et al., 2010; Manning and Dyer, 2007; Manning and Schoellhamer, 2013), and a floc diameter of 160 m has been often used to distinguish between microflocs and Macroflocs groups (Manning and Dyer, 2002; Manning, 2004; Manning et al., 2010). In order to obtain more general understanding on the floc physical properties, a summary of mean floc properties for the entire floc population and sub-population categorized into

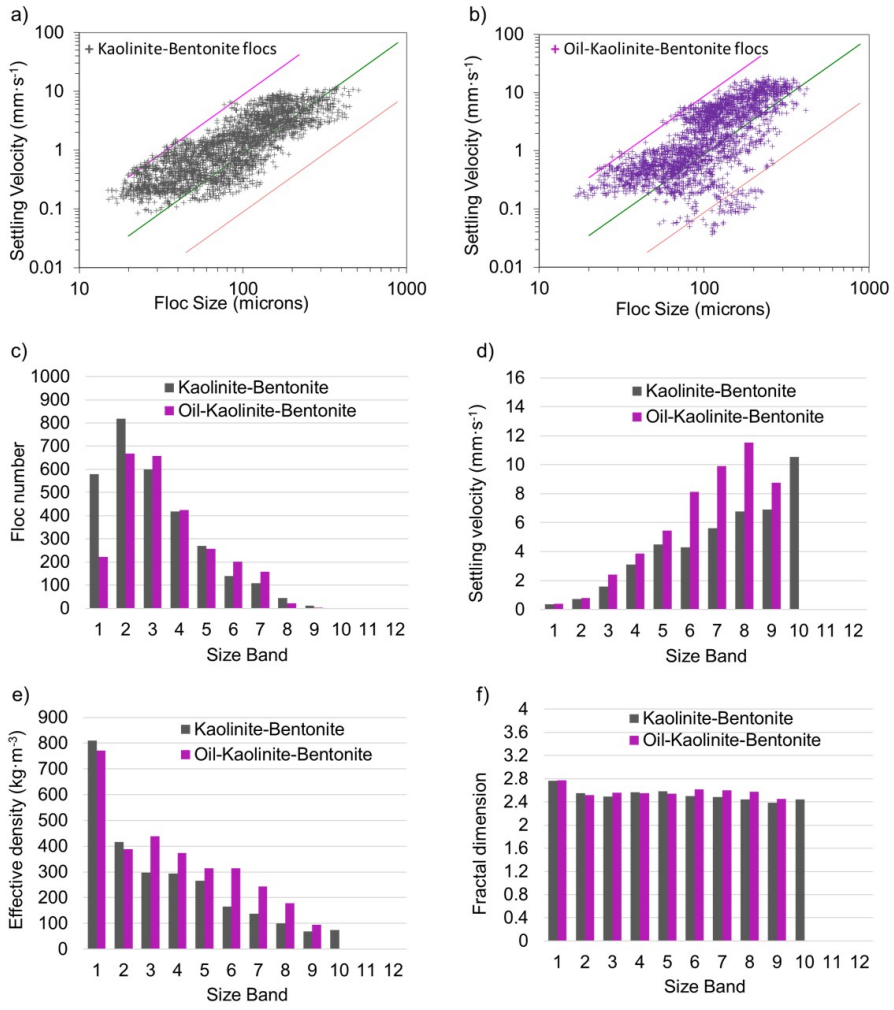

Size Band	1	2	3	4	5	6	7	8	9	10	11	12
Size Range (μm)	20-40	40-80	80-120	120-160	160-200	200-240	240-320	320-400	400-480	480-560	560-640	>640

Figure 7: Floc characteristics from the LabSFLOC-2 analysis. a) & b) show the plots of floc sizes vs. settling velocities of mixed Kaolinite-Bentonite (S05) and Oil-Kaolinite-Bentonite (S06), respectively. The three diagonal lines present contours of Stokes settling velocity calculated with a constant effective density (i.e. floc bulk density minus water density) of 1,600 kg·m^{-3} (pink line, equivalent to a quartz particle), 160 kg·m^{-3} (green) and 16 kg·m^{-3} (red line). c)-f) show the 12 Size Bands trends of floc number, settling velocity, floc density and fractal dimensions respectively for both mixed Kaolinite-Bentonite (blue) and Oil-Kaolinite-Bentonite (orange) samples.

Table 2: Summary of microfloc and Macrofloc mean quantities of each sample investigated in this study.

Samples	Kaolinite			Bentonite			Kaolinite-Bentonite		
Demarcation	Total	micro	Macro	Total	micro	Macro	Total	micro	Macro
N	2631	2128	503	1705	681	1024	2998	2420	578
$\bar{D}(\mu\text{m})$	120	101	199	185	105	238	104	76	225
$\overline{\rho_e}(\text{kg}\cdot\text{m}^{-3})$	315	336	224	127	187	87	410	461	200
$\overline{W_s}(\text{mm}\cdot\text{s}^{-1})$	2.41	1.82	4.89	2.00	1.08	2.61	1.97	1.27	4.90
$\overline{f_n}$	2.54	2.54	2.55	2.30	2.30	2.30	2.57	2.59	2.53

Samples	Oil-Kaolinite			Oil-Bentonite			Oil-Kaolinite-Bentonite		
Demarcation	Total	micro	Macro	Total	micro	Macro	Total	micro	Macro
N	3102	2696	406	1592	580	1012	2610	1975	635
$\bar{D}(\mu\text{m})$	102	86	204	198	115	246	120	87	222
$\overline{\rho_e}(\text{kg}\cdot\text{m}^{-3})$	249	269	113	127	167	104	408	446	290
$\overline{W_s}(\text{mm}\cdot\text{s}^{-1})$	1.21	1.03	2.41	2.53	1.07	3.36	3.33	1.94	7.63
$\overline{f_n}$	2.40	2.40	2.36	2.33	2.29	2.35	2.57	2.57	2.58

microflocs and Macroflocs for all cases are presented in Table 2. Similar to the previous section, the physical floc properties of interest here are floc number (N), mean floc size ($\bar{D}$), mean effective density ($\overline{\rho_e}$), mean settling velocity ($\overline{W_s}$) and mean fractal dimensions ($\overline{f_n}$).

3.3.1. Mineral types influence on flocculation

A comparison between Kaolinite (S01) and Bentonite flocs (S03) show that the Kaolinite flocs in total have around 35 % higher N (2631 versus 1705) and 35 % smaller$\bar{D}$ (120 versus 185 μm) (see Table 2). Moreover, the larger N in Kaolinite is only due to microflocs and Kaolinite has only half of

that of Bentonite in terms of Macrofloc numbers. This matches with the previous clay flocculation studies in saline water (e.g., Zhang et al. 2019). Due to the water salinity, the attraction forces (London-van der Waals' forces) between the clay plates can be dramatically enhanced over repulsion forces. Particularly for Bentonite clay, the enhancement of flocculation can be significantly larger than Kaolinite does under the same salinity which results in more Macroflocs forming in Bentonite case. The $\overline{\rho_e}$ for the entire floc population of Kaolinite floc is around 2.5 times higher than that of Bentonite floc. This is particularly due to the Macroflocs with significantly low $\overline{\rho_e}$ (only 87 kg·m^{-3}) in Bentonite with a mean density of only 87 kg·m^{-3}. Despite somewhat smaller $\bar{D}$ of Kaolinite flocs, their significantly larger $\overline{\rho_e}$ results in approximately 20 % larger $\overline{W_s}$ than that of Bentonite flocs. Finally, $\overline{f_n}$ of Kaolinite flocs is about 2.54, which is higher than that of Bentonite flocs of around 2.3. The differences of Kaolinite and Bentonite flocs revealed here can be directly link to the different types of mineral particle stickiness in saline water (see Figure 3) which shows Bentonite have almost five times higher R_f than that of Kaolinite in the seawater of 35 ppt. Even with the much lower salinity condition (1.2∼3.5 ppt, tested by Khelifa et al. (2005b)), the clay types still can be a significant factor for influencing the flocculation.

The microfloc $\bar{D}$ in the mixed sample is 15 % smaller than that of Kaolinite, and yet in terms of the Macrofloc $\bar{D}$, mixed sample is 13 % larger. In fact, the Macrofloc $\bar{D}$ for mixed Kaolinite-Bentonite sample is nearly comparable (only 5 % smaller) to that of pure Bentonite. Although the

resulting $\overline{W_s}$ of mixed Kaolinite-Bentonite sample for the whole floc population (1.97 mm·s^{-1}) is very similar to that of pure Bentonite sample (2.0 mm·s^{-1}), the mixed sample reaches the similar $\overline{W_s}$ due to having the largest $\overline{\rho_e}$ (410 kg·m^{-3}) and the smallest $\bar{D}$ (104 microns) comparing with those of the two pure clay samples. Looking more into the difference, we can see that Macrofloc $\bar{D}$ and Macrofloc $\overline{\rho_e}$ of Kaolinite-Bentonite mixture is about 13 % larger and 12 % smaller than those of pure Kaolinite sample, respectively, which suggests a slight increase of cohesion in Kaolinite-Bentonite flocs, possibly due to the presence of Bentonite. In terms of microflocs, Kaolinite-Bentonite sample show the smallest and the densest flocs which is also more similar to the microfloc of pure Kaolinite sample, but distinctly different from those of pure Bentonite sample. Moreover, examining the $\bar{D}$ of mixed Kaolinite-Bentonite sample further reveals distinct behavior between microflocs and Macroflocs. The mixture sample possesses a dual feature, namely, the Kaolinite behavior in microflocs and Bentonite behavior in Macroflocs. When mixing two types mineral, the Macroflocs development is slightly enhanced by the more cohesive Bentonite component, but for the entire mixed floc characteristics the effect of Bentonite appears to be benign while the effect of Kaolinite appears to be dominant, especially in microfloc population. This seemingly subtle point between Bentonite and Kaolinite is raised here because it may play a more important role when interacting with oil droplets. Particularly for the oil spilled occurring in natural mixture sediment environment, each clay type influence should be fully understood

necessarily.

3.3.2. Oil participation in mineral flocculation

By adding oil component to the Kaolinite floc sample (S02 in Table 1), oil-Kaolinite N for the entire population increases by around 18 % while the corresponding $\bar{D}$ decreases by around 18 %. However, instead of obtaining a slight increase of $\overline{\rho_e}$ commonly occurs due to decreased cohesion, the $\overline{\rho_e}$ for the entire population also decreases by 20 %. As a result of both reduced $\bar{D}$ and $\overline{\rho_e}$, we obtain a significant reduction of $\overline{W_s}$ by 50 % (decreases from 2.41 mm·s^{-1} to 1.21 mm·s^{-1}, see Table2). Looking further into the microfloc and Macrofloc statistics, we observe different response of microfloc and Macrofloc due to the addition of oil to Kaolinite in the saline water. The microfloc population shows a 27 % increase in N and 15 % reduction of $\bar{D}$, while the Macrofloc population show 20 % reduced in N and very slight 2.5 % increase (or nearly unchanged) $\bar{D}$. This indicates a small shift to microflocs and reduction of cohesion (flocculation rate) due to the addition of oil. The common and more significant trend for both microfloc and Macrofloc is their reduction of $\overline{\rho_e}$: the microflocs show slight (20 %) decrease of $\overline{\rho_e}$ while the Macroflocs show nearly a factor 2 decrease of $\overline{\rho_e}$. As a result, the microfloc and Macrofloc $\overline{W_s}$ are decreased by 43 % and 51 %, respectively. Overall, the participation of lower density oil droplets reduces the OMA density, consistent with the droplet OMA structure presented in Figure 4. The settling velocity data in Table 2 confirms that pure Kaolinite flocs tend to attach

with the oil droplets (around the surface) forming OMAs with much lower density than the original pure Kaolinite mineral flocs.

For Bentonite clay, adding oil component decreases total N by around 7 % while $\bar{D}$ for the entire floc population increases by around 7 %. On the other hand, although the $\overline{\rho_e}$ for the entire floc population is unchanged by adding oil, we obtain 11 % decrease of microfloc $\overline{\rho_e}$ while the Macrofloc $\overline{\rho_e}$ is increased more significantly by 20 %. As a result, microfloc $\overline{W_s}$ is nearly unchanged while the Macrofloc $\overline{W_s}$ is increased by 29 %. Since the total flocs are dominated by Macroflocs in the Bentonite cases, the $\overline{W_s}$ for the entire population is increased by 25 % when adding oil mainly and this is caused by the increase of $\overline{\rho_e}$ in Macroflocs.

By adding oil into mixed Kaolinite-Bentonite clay (S06), the total N shows a reduction of around 13 %, and total $\bar{D}$ increases by around 15 %. Adding oil decreases microfloc N by 18 % and increases microfloc $\bar{D}$ by 14 %. Oil also causes the Macrofloc N to increase by 10 % but with negligible decrease of $\bar{D}$. Consistent with adding oil to pure Bentonite, here we see a 45 % increase in $\overline{\rho_e}$ of Macrofloc by adding oil to mixed Kaolinite-Bentonite sample. As a result, $\overline{W_s}$ increases almost 70 % due to the minor increase of microfloc $\bar{D}$ as well as more dramatic increase of $\overline{\rho_e}$ in Macroflocs.

4. Discussion

The results presented above indicate unique differences of floccualtion characteristics between Kaolinite and Bentonite OMAs which may be closely

influenced by the OMA structures. Previously, this hasn't been clearly revealed by studying the natural mixture sediment samples directly (e.g., Khelifa et al. 2005b, 2008; Sun et al. 2010, 2013; O'Laughlin et al. 2017). Kaolinite particles tend to show lower cohesion and the resulting oil-Kaolinite aggregates can be categorized as droplet OMAs. The pickering emulsions (Chevalier and Bolzinger, 2013) may apply to the oil-Kaolinite droplets flocs in terms of the single droplet OMA structures (e.g., Figure 4a_2). But the Kaolinite OMA also can be a bit more complex when multiple mineral flocs and oil droplets can also possibly attach together and combine to larger aggregates. In this case, the mineral clay particles/flocs adhere on the oil droplets surface, and the mineral particles act as a web-structures surrounding the oil droplet preventing its attachment to other oil droplets or further re-bonding to oil slicks. Previous studies (e.g.,Zhao et al. 2017) have found that equilibrium droplet oil-sediment aggregates can be considered as very stable structure and hardly breakup. Since the Kaolinite mineral particles can be attached together as a much larger structure than individual oil droplet, the oil can be observed being attached or even embraced within the Kaolinite flocs (Figure 4a_{2-4}). Because oil droplets structure remains intact, the oil-Kaolinite OMAs show significantly lower effective density and settling velocity than the pure Kaolinite flocs. This also apply to the natural clay mineral formed mixture oil sediment aggregates according to Khelifa et al. (2008) suggesting that oil-sediment aggregates have 2 to 3 times lower effective density than pure sediment flocs because of the low density oil droplets

attaching within the flocs. On the other hand, Bentonite particles are of very high cohesion and are observed to form large, fluffy (low density and high porosity) and complex aggregate structure. The Bentonite aggregates tend to re-shape and absorb or be absorbed by the oil droplets forming large (as large as 900 microns floc has been observed) dense oil-Bentonite aggregates (Figure 4b_{2-4}). Previous experimental work also indicates that the oil-sediment aggregates formed using natural sediment can be as large as 900 microns (O'Laughlin et al., 2017) and their settling velocity can be variable depending on oil amount trapped in sediment mixture aggregates (Sun et al., 2010). They also suggest that higher sediment concentration may lead to larger flocs with higher settling velocity. In the results presented here further specify the clay type influence to the oil-sediment aggregates' characteristics. Particularly for the Bentonite clay, because the oil droplets no longer exists by themselves and the oil is mainly absorbed at micro-scale level onto the mineral structure, the Bentonite particles can actually become more compact together than its pure mineral floc structure (high porosity) and the resulting OMAs are dominated by denser and larger Macroflocs. The overall settling velocities of oil-Bentonite OMAs are also slightly larger than the pure Bentonite flocs. The response of Kaolinite and Bentonite to the addition of oil are distinctly different due to the corresponding droplet OMA and flake/solid OMA structures, respectively. Overall, in Kaolinite, oil significantly decreases effective density and hence the settling velocity decreases significantly for the entire floc population. Meanwhile, oil slightly increases

693 settling velocity of oil-Bentonite flocs due to increasing floc size and effective
694 density in Macrofloc population. Therefore, adding oil into pure Kaolin-
695 ite has negative influence to the cohesion and flocculation which agrees with
696 Khelifa et al. (2008). However, the cohesion of Bentonite can be increased by
697 oil participation because of its unique high porous structure. The stickiness
698 (cohesion) can be one of the most significant key factor for the OMA floc-
699 culation. Since chemical dispersant may increase the oil droplets stickiness
700 to enhance the oil-sediment flocculation after oil spill occourance in natural
701 enviornment (Khelifa et al. 2008), the higher stickiness of bentonite clay also
702 may have the similar effect on OMA flocculation positively. The significant
703 of stickiness influence may also change the relationship between turbulence
704 level and floc size. Noticeably, both previous study (e.g., Sun et al. (2010,
705 2013)) and present study show that in very high turbulence level, turbulent
706 Kolmogorov length scale has limited effect to the oil-mineral floc size.

707 Furthermore, by adding oil to mixture sample, oil selectively interacts
708 more actively with Bentonite in Macroflocs rather than with Kaolinite under
709 a condition of same amount of clay, respectively. The increase of total floc
710 size and decrease in total floc number by adding oil in the mixed Kaolinite-
711 Bentonite sample (Table 2) indicate a slight enhance of floc cohesion due to
712 the addition of oil. However, a more careful observation suggests that the
713 changes due to the addition of oil are completely different between microfloc
714 and Macrofloc populations especially in the more significant changes of floc
715 effective density which directly leads to the settling dynamics difference.

Overall, adding oil transforms the Macroflocs into higher density OMAs with higher settling velocity due to high stickiness Bentonite component. Moreover, oil also increases the density and settling velocity in microflocs dominant by Kaolinite component with less oil participation. Therefore, with the multiple mixed mineral types exist in the natural environments commonly, their own flocculation capability and settling behaviors may vastly different especially when meeting with other contaminant materials such as spilled oil because the third participation during the mineral flocculation processes may totally change the structures of flocs which may directly influence the flocs characteristics such as porosity, density and most importantly settling velocities.

5. Conclusions

To conclude, the LabSFLOC-2 system has been utilized in OMAs studies to understand flocculation characteristics and settling velocities. Droplet OMAs and flake/solid OMAs have been observed in OMA generation which matches with the previous studies. Furthermore, multiple OMAs structures have been studied. For the mixed oil-Kaolin-Bentonite case which is closer to the natural sediment mixture condition, both Kaolin and Bentonite component can be aggregated with oil droplets and develop OMAs to settling. However, Bentonite becomes more dominate in OMA flocculation efficiency compare with Kaolinite especially in Macrofloc group. From the size-class results, specific size ranges of OMAs can be known when influenced by min-

eral particles or oil component participating in their flocculation. Since the Bentonite clay is one of the most common mineral particles in natural environments, its role in absorbing oil, forming OMAs and influencing the fate of oil need to be incorporated in future modeling efforts.

Acknowledgement

This research was funded by the Gulf of Mexico Research Initiative to CSOMIO project (Grant number:SA18-10). Data are publicly available through the Gulf of Mexico Research Initiative Information and Data Cooperative (GRIIDC) at http://data.gulfresearchinitiative.org.

References

Ainsworth, C.H., Paris, C.B., Perlin, N., Dornberger, L.N., Patterson III, W.F., Chancellor, E., Murawski, S., Hollander, D., Daly, K., Romero, I.C., 2018. Impacts of the deepwater horizon oil spill evaluated using an end-to-end ecosystem model. PloS one 13, e0190840.

Ajijolaiya, L.O., Hill, P.S., Khelifa, A., Islam, R.M., Lee, K., 2006. Laboratory investigation of the effects of mineral size and concentration on the formation of oil–mineral aggregates. Marine pollution bulletin 52, 920–927.

Almeda, R., Connelly, T.L., Buskey, E.J., 2016. How much crude oil can zooplankton ingest? estimating the quantity of dispersed crude oil defecated by planktonic copepods. Environmental pollution 208, 645–654.

758 Almeda, R., Wambaugh, Z., Wang, Z., Hyatt, C., Liu, Z., Buskey, E.J.,
759 2013. Interactions between zooplankton and crude oil: toxic effects and
760 bioaccumulation of polycyclic aromatic hydrocarbons. PloS one 8, e67212.

761 Atlas, R.M., Hazen, T.C., 2011. Oil biodegradation and bioremediation:
762 a tale of the two worst spills in us history. Environmental Science &
763 Technology 45, 6709–6715.

764 Benson, T., Manning, A., 2013. Digifloc: The development of semi-automatic
765 software to determine the size and settling velocity of flocs, in: HR Walling-
766 ford Report DDY0427-RT001.

767 Chanton, J., Zhao, T., Rosenheim, B.E., Joye, S., Bosman, S., Brunner, C.,
768 Yeager, K.M., Diercks, A.R., Hollander, D., 2014. Using natural abundance
769 radiocarbon to trace the flux of petrocarbon to the seafloor following the
770 deepwater horizon oil spill. Environmental science & technology 49, 847–
771 854.

772 Chevalier, Y., Bolzinger, M.A., 2013. Emulsions stabilized with solid
773 nanoparticles: Pickering emulsions. Colloids and Surfaces A: Physico-
774 chemical and Engineering Aspects 439, 23–34.

775 Crone, T.J., Tolstoy, M., 2010. Magnitude of the 2010 gulf of mexico oil leak.
776 Science 330, 634–634.

777 Daly, K.L., Passow, U., Chanton, J., Hollander, D., 2016. Assessing the

impacts of oil-associated marine snow formation and sedimentation during and after the deepwater horizon oil spill. Anthropocene 13, 18–33.

Doshi, B., Sillanpää, M., Kalliola, S., 2018. A review of bio-based materials for oil spill treatment. Water research 135, 262–277.

Engel, A., 2000. The role of transparent exopolymer particles (tep) in the increase in apparent particle stickiness (α) during the decline of a diatom bloom. Journal of Plankton Research 22, 485–497.

Gratiot, N., Manning, A., 2004. An experimental investigation of floc characteristics in a diffusive turbulent flow. Journal of Coastal Research , 105–113.

Guyomarch, J., Le Floch, S., Merlin, F.X., 2002. Effect of suspended mineral load, water salinity and oil type on the size of oil–mineral aggregates in the presence of chemical dispersant. Spill Science & Technology Bulletin 8, 95–100.

Hayakawa, K., Nomura, M., Nakagawa, T., Oguri, S., Kawanishi, T., Toriba, A., Kizu, R., Sakaguchi, T., Tamiya, E., 2006. Damage to and recovery of coastlines polluted with c-heavy oil spilled from the nakhodka. Water Research 40, 981–989.

Henkel, J.R., Sigel, B.J., Taylor, C.M., 2012. Large-scale impacts of the deepwater horizon oil spill: Can local disturbance affect distant ecosystems through migratory shorebirds? BioScience 62, 676–685.

Hill, P., Khelifa, A., Lee, K., 2002. Time scale for oil droplet stabilization by mineral particles in turbulent suspensions. Spill Science & Technology Bulletin 8, 73–81.

Huang, C.J., Ma, H., Guo, J., Dai, D., Qiao, F., 2018. Calculation of turbulent dissipation rate with acoustic doppler velocimeter. Limnology and Oceanography: Methods 16, 265–272.

Jones, A.N., Bridgeman, J., 2016. Investigating the characteristic strength of flocs formed from crude and purified hibiscus extracts in water treatment. Water research 103, 21–29.

Khelifa, A., Fingas, M., Brown, C., 2008. Effects of dispersants on oil-spm aggregation and fate in us coastal waters. Final Report Grant Number: NA04NOS4190063 .

Khelifa, A., Hill, P.S., Lee, K., 2005a. The role of oil-sediment aggregation in dispersion and biodegradation of spilled oil, in: Developments in Earth and Environmental Sciences. Elsevier. volume 3, pp. 131–145.

Khelifa, A., Stoffyn-Egli, P., Hill, P.S., Lee, K., 2002. Characteristics of oil droplets stabilized by mineral particles: effects of oil type and temperature. Spill Science & Technology Bulletin 8, 19–30.

Khelifa, A., Stoffyn-Egli, P., Hill, P.S., Lee, K., 2005b. Effects of salinity and clay type on oil–mineral aggregation. Marine environmental research 59, 235–254.

Le Floch, S., Guyomarch, J., Merlin, F.X., Stoffyn-Egli, P., Dixon, J., Lee, K., 2002. The influence of salinity on oil–mineral aggregate formation. Spill Science & Technology Bulletin 8, 65–71.

Lee, K., Stoffyn-Egli, P., 2001. Characterization of oil-mineral aggregates, in: International Oil Spill Conference, American Petroleum Institute. pp. 991–996.

Liu, Z., Callies, U., 2019. A probabilistic model of decision making regarding the use of chemical dispersants to combat oil spills in the german bight. Water Research , 115196.

Liu, Z., Liu, J., Zhu, Q., Wu, W., 2012. The weathering of oil after the deep-water horizon oil spill: insights from the chemical composition of the oil from the sea surface, salt marshes and sediments. Environmental Research Letters 7, 035302.

Loh, A., Shim, W.J., Ha, S.Y., Yim, U.H., 2014. Oil-suspended particulate matter aggregates: Formation mechanism and fate in the marine environment. Ocean Science Journal 49, 329–341.

Manning, A., 2004. The observed effects of turbulence on estuarine flocculation. Journal of Coastal Research SI 41, 90–104.

Manning, A., Dyer, K., 2007. Mass settling flux of fine sediments in northern european estuaries: measurements and predictions. Marine Geology 245, 107–122.

841 Manning, A., Schoellhamer, D., 2013. Factors controlling floc settling velocity
842 along a longitudinal estuarine transect. Marine Geology 345, 266–280.

843 Manning, A.J., Baugh, J.V., Spearman, J.R., Whitehouse, R.J., 2010. Floc-
844 culation settling characteristics of mud: sand mixtures. Ocean dynamics
845 60, 237–253.

846 Manning, A.J., Dyer, K.R., 2002. The use of optics for the in situ determi-
847 nation of flocculated mud characteristics. Journal of Optics A: Pure and
848 Applied Optics 4, S71.

849 Murawski, S.A., Hogarth, W.T., Peebles, E.B., Barbeiri, L., 2014. Preva-
850 lence of external skin lesions and polycyclic aromatic hydrocarbon concen-
851 trations in gulf of mexico fishes, post-deepwater horizon. Transactions of
852 the American Fisheries Society 143, 1084–1097.

853 O'Laughlin, C.M., Law, B.A., Zions, V.S., King, T.L., Robinson, B., Wu, Y.,
854 2017. Settling of dilbit-derived oil-mineral aggregates (omas) & transport
855 parameters for oil spill modelling. Marine pollution bulletin 124, 292–302.

856 Omotoso, O.E., Munoz, V.A., Mikula, R.J., 2002. Mechanisms of crude
857 oil–mineral interactions. Spill Science & Technology Bulletin 8, 45–54.

858 Passow, U., 2002. Transparent exopolymer particles (tep) in aquatic envi-
859 ronments. Progress in oceanography 55, 287–333.

860 Passow, U., Hetland, R.D., 2016. What happened to all of the oil? Oceanog-
861 raphy 29, 88–95.

862 Passow, U., Ziervogel, K., Asper, V., Diercks, A., 2012. Marine snow for-
863 mation in the aftermath of the deepwater horizon oil spill in the gulf of
864 mexico. Environmental Research Letters 7, 035301.

865 Peterson, C.H., Rice, S.D., Short, J.W., Esler, D., Bodkin, J.L., Ballachey,
866 B.E., Irons, D.B., 2003. Long-term ecosystem response to the exxon valdez
867 oil spill. Science 302, 2082–2086.

868 Reddy, C.M., Arey, J.S., Seewald, J.S., Sylva, S.P., Lemkau, K.L., Nelson,
869 R.K., Carmichael, C.A., McIntyre, C.P., Fenwick, J., Ventura, G.T., 2012.
870 Composition and fate of gas and oil released to the water column during
871 the deepwater horizon oil spill. Proceedings of the National Academy of
872 Sciences 109, 20229–20234.

873 Reddy, C.M., Eglinton, T.I., Hounshell, A., White, H.K., Xu, L., Gaines,
874 R.B., Frysinger, G.S., 2002. The west falmouth oil spill after thirty years:
875 the persistence of petroleum hydrocarbons in marsh sediments. Environ-
876 mental science & technology 36, 4754–4760.

877 Romero, I.C., Toro-Farmer, G., Diercks, A.R., Schwing, P., Muller-Karger,
878 F., Murawski, S., Hollander, D.J., 2017. Large-scale deposition of weath-
879 ered oil in the gulf of mexico following a deep-water oil spill. Environmental
880 pollution 228, 179–189.

881 Shen, X., Lee, B.J., Fettweis, M., Toorman, E.A., 2018. A tri-modal floccula-

tion model coupled with telemac for estuarine muds both in the laboratory and in the field. Water research 145, 473–486.

Sterling Jr, M.C., Bonner, J.S., Ernest, A.N., Page, C.A., Autenrieth, R.L., 2005. Application of fractal flocculation and vertical transport model to aquatic sol–sediment systems. Water research 39, 1818–1830.

Stoffyn-Egli, P., Lee, K., 2002. Formation and characterization of oil–mineral aggregates. Spill Science & Technology Bulletin 8, 31–44.

Stokes, G.G., 1851. On the effect of the internal friction of fluids on the motion of pendulums. volume 9. Pitt Press Cambridge.

Strom, K., Keyvani, A., 2016. Flocculation in a decaying shear field and its implications for mud removal in near-field river mouth discharges. Journal of Geophysical Research: Oceans 121, 2142–2162.

Sun, J., Khelifa, A., Zheng, X., Wang, Z., So, L.L., Wong, S., Yang, C., Fieldhouse, B., 2010. A laboratory study on the kinetics of the formation of oil-suspended particulate matter aggregates using the nist-1941b sediment. Marine pollution bulletin 60, 1701–1707.

Sun, J., Zhao, D., Zhao, C., Liu, F., Zheng, X., 2013. Investigation of the kinetics of oil–suspended particulate matter aggregation. Marine pollution bulletin 76, 250–257.

Uncles, R., Mitchell, S., 2017. Estuarine and coastal hydrography and sediment transport. Cambridge University Press.

Voulgaris, G., Trowbridge, J.H., 1998. Evaluation of the acoustic doppler velocimeter (adv) for turbulence measurements. Journal of atmospheric and oceanic technology 15, 272–289.

White, H.K., Hsing, P.Y., Cho, W., Shank, T.M., Cordes, E.E., Quattrini, A.M., Nelson, R.K., Camilli, R., Demopoulos, A.W., German, C.R., 2012. Impact of the deepwater horizon oil spill on a deep-water coral community in the gulf of mexico. Proceedings of the National Academy of Sciences 109, 20303–20308.

Winterwerp, J.C., Van Kesteren, W.G., 2004. Introduction to the physics of cohesive sediment dynamics in the marine environment. volume 56. Elsevier.

Yan, B., Passow, U., Chanton, J.P., Nöthig, E.M., Asper, V., Sweet, J., Pitiranggon, M., Diercks, A., Pak, D., 2016. Sustained deposition of contaminants from the deepwater horizon spill. Proceedings of the National Academy of Sciences 113, E3332–E3340.

Zhang, T., Deng, Y., Cui, Y., Lan, H., Zhang, F., Zhang, H., 2019. Porewater salinity effect on flocculation and desiccation cracking behaviour of kaolin and bentonite considering working condition. Engineering geology 251, 11–23.

Zhao, L., Boufadel, M.C., Geng, X., Lee, K., King, T., Robinson, B., Fitz-

patrick, F., 2016. A-drop: A predictive model for the formation of oil particle aggregates (opas). Marine pollution bulletin 106, 245–259.

Zhao, L., Boufadel, M.C., King, T., Robinson, B., Gao, F., Socolofsky, S.A., Lee, K., 2017. Droplet and bubble formation of combined oil and gas releases in subsea blowouts. Marine pollution bulletin 120, 203–216.

Zhao, L., Torlapati, J., Boufadel, M.C., King, T., Robinson, B., Lee, K., 2014. Vdrop: A comprehensive model for droplet formation of oils and gases in liquids-incorporation of the interfacial tension and droplet viscosity. Chemical Engineering Journal 253, 93–106.